DOI: 10.13009/EUCASS2023-374
Aerospace Europe Conference 2023 – 10TH EUCASS – 9TH CEAS

Derivation and Verification of a Flexible Hexapod Model for Multi-Body Space Observatories

Alison Ponche[⋆†], *Andrés Marcos*[⋆], *Thomas Ott*[⋆⋆], *Ramin Geshnizjani*[⋆⋆]

[⋆]*University Carlos III de Madrid (UC3M)*
Juan Benet Building, Av. de la Universidad 30, 28911, Leganes, Spain
aponche@pa.uc3m.es · anmarcos@ing.uc3m.es

[⋆⋆]*Airbus Defence and Space GmbH*
Claude-Dornier-Strasse 1, 88090 Immenstaad, Germany
thomas.ott@airbus.com · ramin.geshnizjani@airbus.com

[†]Corresponding author

Abstract

In order to provide the high-accuracy pointing objectives required by recent and future space telescope scientific missions, complex mechanisms such as hexapods are being proposed to move the primary telescope mirrors in six degrees of freedom. Such hexapod mechanisms are expected to have stiffness and damping properties that will interact with the spacecraft flexible modes resulting in potential loss of performance. Thus, it is critical to obtain appropriate design and analysis mathematical models of the complete flexible multi-body system. In this article, a direct method that avoids iterative computations is proposed to derive a stiffness model for such a multi-body / multi-actuator telescope mirror spacecraft. An industrial, high-fidelity multi-body dynamic simulator is used to assess the derived model, and the results show its validity.

1. Introduction

Recent space telescopes are large complex multi-body and multi-actuator spacecraft, enabling to observe the same target successively with different on-board instruments by using a common and large movable focusing device (named primary mirror). Examples are the current James Webb Space Telescope and the future Advanced Telescope for High-Energy Astrophysics (ATHENA). They both use a hexapod as a high-accuracy pointing mechanism to orient their primary mirror in six degrees of freedom. With the movable mass amounting to up to 20% of the total spacecraft mass, multi-body/multi-actuator spacecraft pose new challenges for the attitude and line of sight control. Indeed, this high mass ratio combined with the low inertia of the hexapod's actuators induces flexibility between the rigid main-body and the rigid mirror. At the multi-body level, these flexible modes could interact with the ones from the appendages (e.g. the solar arrays). In addition, disturbances from the actuators motors could excite these interacting flexible modes. Thus, a flexible mode analysis of the whole spacecraft has become necessary to assess if any flexible mode will be excited during a combined hexapod motion and spacecraft attitude maneuver. As a first step, an equivalent stiffness model of the hexapod depending explicitly on the hexapod characteristics is needed. Hence, the focus of this work is to derive a suitable design model such that these effects can be considered in the attitude controller synthesis.

Especially for high-accuracy pointing modes, the ACS can be designed and analyzed using linear models that relate forces and torques to linear and angular displacements. For common flexible appendages such as solar arrays or antennas, explicit state-space models are usually derived with direct access to modal parameters.[11] In turn, these models can directly be fed with reliable modal analysis results. Unlike these serial appendages, hexapod mechanisms contain closed-loop kinematic chains between their base and their moving platform. This is due to the multiple joints that are linked to the same body, adding algebraic constraints to the system of differential equations. Thus, these mechanisms are ruled by differential-algebraic equations, making them highly non-linear. Their dynamic modeling is not straightforward and requires solving the kinematics and dynamics problems, and thus no explicit linear models are available.

In the rigid case, the forward and inverse kinematics problem has been widely tackled and solved during the 1990's, under geometrical or additional sensing assumptions.[18,23] This enables relating accurately the platform states (i.e. position, orientation and derivatives) to the actuators' states (i.e. length and derivatives), and vice-versa. Solving

DOI: 10.13009/EUCASS2023-374

the inverse dynamics problem and combining the solution to the kinematics solution enables relating the forces and torques exerted on the platform to its states (i.e. acceleration, velocity and position). Two approaches are used to solve the dynamics problem: the Newtonian approach explicitly derives all forces and torques acting on the individual bodies,[5,6] while the Lagrangian approach leads to a set of equations in function of the generalized coordinates.[8] Later, the need of simplified models to solve such dynamics in real-time arose, and modern approaches led to faster convergence than the classical ones. Notable ones are based on the principle of virtual work[24] to force the loop closure constraints, on the generalized momentum approach.[15] One of the original methods to derive a flexible hexapod dynamical model is to include the legs and/or joints flexibility in the rigid formulation.[10,13] All these methods are exact and therefore nonlinear. Thus, they are more adapted to simulating high-fidelity non-linear models than obtaining control design models.

More recently, the focus changed from the dynamics formulation and the non-linear modeling towards linear modeling and control. Alazard, Sanfedino et al. derive linear models using their direct dynamic TITOP approach.[3,21] This approach combines the structure and control fields by embedding the first natural frequencies and modal shapes of each flexible body in the global dynamics model. So far, this method has been applied to many multi-body spacecraft with serial appendages[22] (i.e. in a chain-like and tree-like multi-body systems) and to simple closed-loop kinematic chain systems.[4,7] However, the method does not solve the loop closure constraint for larger and more complex closed-loop kinematic chain systems.

A different path was taken by Li et al.[14] for controlling the vibration isolation of a payload with a hexapod mechanism. In this case, the actuators' stiffness is augmented or reduced actively by applying a control force in the legs. The authors compute this control force by estimating the actuators' stiffness with measurements of both the velocity and attitude of the payload and the velocity and attitude of the main body. However, the global flexible behavior of the spacecraft with its appendages is approximated with low- and high-frequency disturbance signals. Thus the method might not manage the real stiffness coupling effects and various flexible modes.

Thus, there is no linear, representative hexapod model that captures its flexible behavior and can be used for control synthesis. This article addresses the aforementioned needs and presents the derivation, verification and validation of an equivalent linear stiffness model for a hexapod. It consists of a 6-by-6 Cartesian stiffness matrix that relates the forces and torques applied on the hexapod's platform to its linear and angular displacements. This global matrix contains the information of both the individual actuators' stiffness properties and the hexapod geometry. This matrix enables computing the flexible modes' frequencies and amplitudes induced by the hexapod in the global spacecraft. This parameterized and simple linear model of the hexapod mechanism offers the possibility to perform a systematic model extension if needed. For example the general damping behavior can be included by following the same method once damping information on the individual actuators will be available. Such a linear model is of high-interest for robust control design and analysis, since its parameters can easily be extended to uncertain parameters.

The article is organized as follows. Section 2 recalls the geometric modeling of hexapod mechanisms on which the following developments are based. Section 3 presents the derivation of the equivalent Cartesian stiffness matrix of the hexapod. The individual actuator stiffness matrices are formulated and aggregated into a global one for the mechanism. The advantage of such a matrix is that it relates the forces and torques acting on the hexapod's platform to its translational and angular displacements. The linear dynamics with this computed stiffness matrix is solved, and the responses to an external wrench on the hexapod's platform are derived. Then, the hexapod equivalent stiffness model is verified and validated in section 4. The process is first applied to a study-case hexapod to obtain an equivalent stiffness matrix. The verification is performed using an Airbus in-house tool for multi-body dynamics. The verification model is derived and contains the equivalent stiffness matrix of the study-case hexapod as interconnection between two bodies. The validation is then performed using the commercially available non-linear simulation tool Simscape Multibody. The validation model contains the six actuators of the study-case hexapod as interconnection between two bodies. Both verification and validation models are simulated and their responses to identical impulsive forces and torques on the platform are compared to the analytical ones. The verification assesses the consistency of the linear dynamics formulation, while the validation assesses the physicality of this equivalent stiffness matrix.

2. Hexapod mechanism and parameterization

Hexapod mechanisms are used to improve the pointing accuracy for current and future science observation missions. In this section a general hexapod mechanism is described in order to motivate the subsequent modeling challenges and complexity of the task.

A hexapod mechanism is composed of a base, an end-platform and a set of extensible leg actuators. The geometrical configuration varies with the spatial arrangement of the legs, i.e. the position of the junction points at the base and the platform. From the literature, it is well-known that a hexapod structure connecting the base and the platform in three pairs is more resistant to external forces and torques acting on the platform since it cancels

DOI: 10.13009/EUCASS2023-374

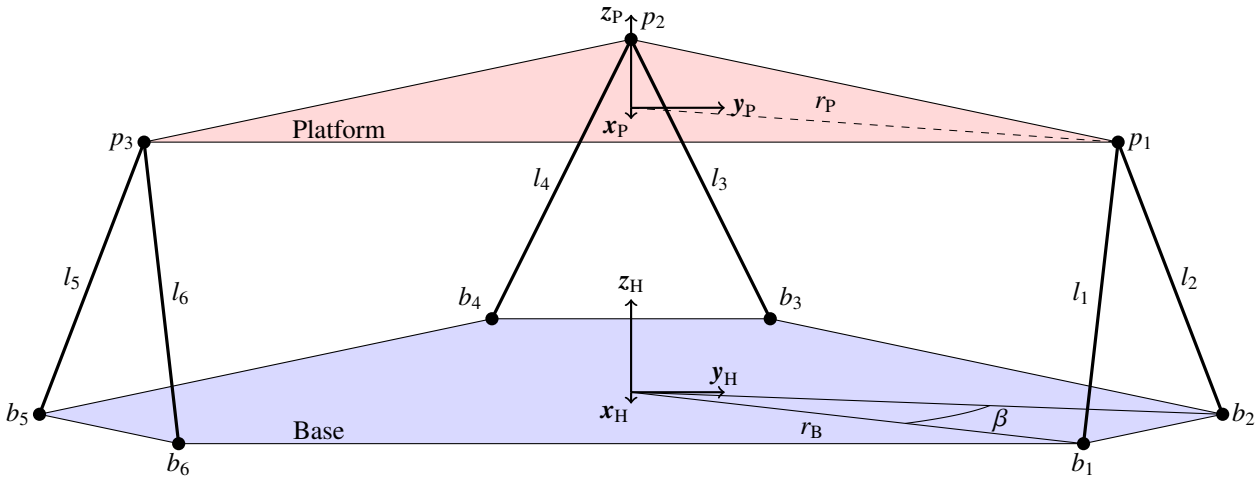

Figure 1: Sketch of the considered 6x3 hexapod mechanism

the free rotation of the platform around the vertical axis of the hexapod.[12] The two missions mentioned above use such a geometry, called 6-3 hexapod geometry. Hence, this article focuses on this geometry and proposes a general parameterization of it in order to develop a systematic stiffness model (see Figure 1).

A frame {P} attached to the moving platform is defined to characterize its position and orientation relatively to the reference hexapod's base frame {H}. The actuator length (l), the radii on base side and platform side (respectively r_B and r_P), and the angle between two nearby base points from base center β characterize the hexapod's geometry.

In addition to the previous parameters, the leg angle from the vertical γ is needed for later frame transformations between the leg and the hexapod's platform. Some supplementary parameters are required to compute this angle and are depicted in Figure 2.

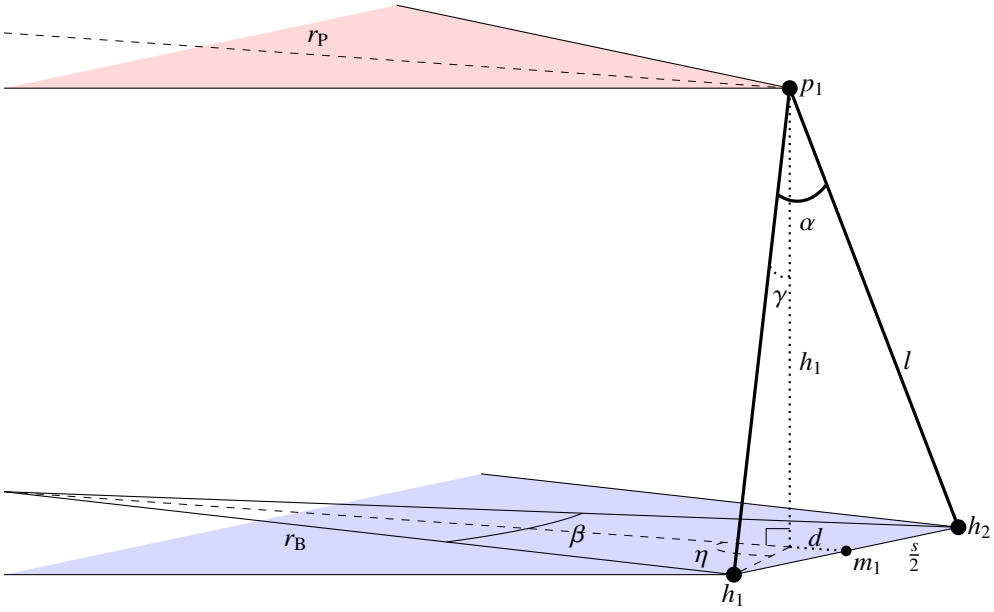

Figure 2: Additional geometric parameters of the 6x3 hexapod

First, the bipod base length s, i.e. the distance between two nearby base points, is given by:

$$s = 2\, r_B \sin\left(\frac{\beta}{2}\right) \tag{1}$$

DOI: 10.13009/EUCASS2023-374

The angle α between two nearby base points from the related platform point can be computed as:

$$\alpha = 2 \arcsin\left(\frac{s/2}{l}\right) \tag{2}$$

In order to compute the projection h_1 of the platform point p_1 to the base, the distance d is used. It is the distance between the platform radius r_P and the middle of the bipod length m_1.

$$d = \sqrt{{r_\mathrm{B}}^2 - \left(\frac{s}{2}\right)^2} - r_\mathrm{P} \tag{3}$$

Now, the distance h_1 can be computed.

$$h_1 = \sqrt{\left(l \cos\left(\frac{\alpha}{2}\right)\right)^2 - d^2} \tag{4}$$

Lastly, the leg angle from the vertical γ can be computed.

$$\gamma = \arccos\left(\frac{h_1}{l}\right) \tag{5}$$

Considering that the i-th leg has for transversal axis $\boldsymbol{z}_i$, then the rotation from the leg frame to the hexapod's platform frame is not unique {P}. Thus, the rotation matrix is defined by using the angle from the positive x_H-axis to the i-th base junction point h_i is (see Figure 1):

$$\theta_i = \begin{cases} \eta_i - \dfrac{\beta}{2} & \text{if } i \in \{1,3,5\} \\ \eta_i + \dfrac{\beta}{2} & \text{if } i \in \{2,4,6\} \end{cases}, \tag{6}$$

where $\eta_1 = \eta_2 = 60°$, $\eta_3 = \eta_4 = 180°$ and $\eta_5 = \eta_6 = 300°$.

Using the θ_i angle, the direction cosine matrix ${}^\mathrm{P}\boldsymbol{R}_{\mathrm{L_i}}$ from the i-th leg local frame $\{\mathrm{L_i}\}$ to the hexapod's platform frame {P} can be defined as in Eq. (7).

$${}^\mathrm{P}\boldsymbol{R}_{\mathrm{L_i}} = R_z(\theta_i)\, R_y(\gamma), \forall i \in [\![1;6]\!] \tag{7}$$

3. Linear model with Hexapod equivalent stiffness matrix

This section presents the derivation of an equivalent stiffness model of the hexapod. It consists in a 6-by-6 Cartesian stiffness matrix that relates the forces and torques applied on the hexapod's platform to its linear and angular displacements. This matrix contains the information on the flexible behavior of a hexapod mechanism and enables computing the flexible modes induced by the hexapod in the global spacecraft.

3.1 Linear dynamics formulation

The non-linear formulation of the dynamics of the hexapod including the actuators' stiffness does not enable a straightforward linearization and thus an adapted model for control. The interest of developing an equivalent 6-by-6 stiffness matrix of the hexapod is that it enables the formulation of an equivalent linear model of the hexapod. Indeed, the 6-by-6 stiffness matrix $\boldsymbol{K}$ of the hexapod relates the external wrench $\boldsymbol{w}_\mathrm{ext}$ (i.e. forces and torques) applied on the platform to the linear and angular displacement $\boldsymbol{x}$ of the platform from its equilibrium pose, at a given point. Let $\boldsymbol{M}$ be the 6-by-6 global mass matrix of the platform.[20] Since it is expressed with respect to the platform's center of mass, this matrix is block-diagonal and contains the mass matrix in the first sub-matrix, and its moment of inertia matrix in the second one. Then, the 6-dof platform motion is governed by the well-known six equations of motion, given in a matrix form in Eq. (8). They relate small perturbations in the platform accelerations $\ddot{\boldsymbol{x}}$ and positions $\boldsymbol{x}$ to external forces and torques applied on the platform. All quantities are expressed at the platform center of mass p and defined in the platform-fixed frame {P}.

$$\boldsymbol{M}\,\ddot{\boldsymbol{x}} + \boldsymbol{K}\,\boldsymbol{x} = \boldsymbol{w}_\mathrm{ext}, \tag{8}$$

For a real physical system, the global mass matrix $\boldsymbol{M}$ is always positive definite.[16] In addition, the specific 6-3 hexapod geometry leads to a non-singular Cartesian stiffness matrix $\boldsymbol{K}$,[19] which makes it also definite positive. This means that it has a stable behavior to an external wrench input.

DOI: 10.13009/EUCASS2023-374

3.2 Impulse response

The global mass matrix $\boldsymbol{M}$ is positive definite and thus has an inverse $\boldsymbol{M}^{-1}$. Therefore, Eq. (8) can be rewritten as:

$$\ddot{\boldsymbol{x}} + \boldsymbol{M}^{-1}\,\boldsymbol{K}\,\boldsymbol{x} = \boldsymbol{M}^{-1}\,\boldsymbol{w}_{\text{ext}} \tag{9}$$

As explained in section 3.1, $\boldsymbol{K}$ is also positive definite, thus the product $\boldsymbol{M}^{-1}\,\boldsymbol{K}$ has positive eigenvalues. Therefore, there exists an invertible matrix $\boldsymbol{P}$ such that:

$$\boldsymbol{P}^{-1}\,\boldsymbol{M}^{-1}\,\boldsymbol{K}\,\boldsymbol{P} = \boldsymbol{D} = \text{diag}\{\lambda_1, \ldots, \lambda_6\}\,, \tag{10}$$

where $\lambda_1, \ldots, \lambda_6 > 0$ are the eigenvalues of $\boldsymbol{M}_{\mathcal{P},\text{P}}^{-1}\,\boldsymbol{K}$. Multiplying Eq. (9) by $\boldsymbol{P}^{-1}$ from the left and inserting Eq. (10) yields the decoupled equations of motion, which are now expressed in the eigenbasis:

$$\ddot{\tilde{\boldsymbol{x}}} + \boldsymbol{D}\,\tilde{\boldsymbol{x}} = \tilde{\boldsymbol{u}} \tag{11}$$

where $\tilde{\boldsymbol{x}} = \boldsymbol{P}^{-1}\,\boldsymbol{x}$ and $\tilde{\boldsymbol{u}} = \boldsymbol{P}^{-1}\,\boldsymbol{M}^{-1}\,\boldsymbol{w}_{\text{ext}}$.

The elements of $\tilde{\boldsymbol{u}}$ are linear combinations of the force and torque inputs along the axes of the {P}-frame. If the system is subjected to impulse inputs, then each element of $\tilde{\boldsymbol{u}}$ is a linear combination of Dirac functions. To compute the impulse response, assume zero initial conditions and transform Eq. (11) into the frequency domain. Then holds Eq. (12):

$$(s^2\,\boldsymbol{I}_3 + \boldsymbol{D})\,\tilde{\boldsymbol{X}}(s) = \tilde{\boldsymbol{U}}\,, \tag{12}$$

where $\tilde{\boldsymbol{U}}$ is the Laplace transform of the input impulse and thus constant. Since $(s^2\,\boldsymbol{I}_3 + \boldsymbol{D})$ is diagonal, Eq. (12) can be inverted element-wise ($i \in \{1, ..., 6\}$) and its solution is:

$$\tilde{X}_i(s) = \frac{u_i}{s^2 + \lambda_i} \tag{13}$$

or in the time domain:

$$\tilde{x}_i(t) = \alpha_i\,\sin(\omega_i\,t) \tag{14}$$

where:

$$\omega_i = \sqrt{\lambda_i} \tag{15}$$

$$\alpha_i = \frac{u_i}{\omega_i} \tag{16}$$

Finally, the solution is transformed back into the R_P frame, where it becomes a linear combination of the eigenmodes:

$$\boldsymbol{x}(t) = \boldsymbol{P}\,\tilde{\boldsymbol{x}}(t) \tag{17}$$

where the i-th element of $\boldsymbol{x}(t)$ is:

$$x_i(t) = \sum_{j=1}^{6} P_{ij}\,\alpha_j\,\sin(\omega_j\,t) \tag{18}$$

3.3 Hexapod equivalent stiffness matrix construction

This section presents a process to construct the stiffness matrix $\boldsymbol{K}$ of the hexapod used in the previous sections, from a single actuator to the aggregated matrix. In the past two decades, the research community has performed an effort to understand and model multi-body systems composed of parallel actuators and rigid bodies, and particularly hexapods. Depending on the research, the community assumes the main contribution of the actuators to the global stiffness is their axial stiffness[17,20] and shows the consistency of the assumption with finite element analyses. This assumption is taken and section 3.3.1 presents a process to derive a 6-by-6 Cartesian stiffness matrix of the actuator: starting from the output of a modal analysis of a single hexapod actuator, each actuator is modeled as a linear spring. The axial stiffness is obtained from the most significant axial mode, since it covers more than 99% of the complete axial behavior over all the axial modes. This axial stiffness is then mapped from the modal coordinates into Cartesian coordinates, leading to a 6-by-6 Cartesian stiffness matrix of the actuator. The advantage of such a matrix is that it relates the forces and torques acting on the actuator to its translational and angular displacements. Then, in section 3.3.2, these individual matrices are aggregated using the hexapod's geometry to form a Cartesian stiffness matrix of the entire hexapod. This matrix is again of dimension 6-by-6 and relates the forces and torques on the hexapod's platform to its linear and angular deflections.

DOI: 10.13009/EUCASS2023-374

3.3.1 Individual actuator 6-by-6 Cartesian stiffness matrix

The goal of this section is to derive a Cartesian stiffness matrix for each leg of the hexapod. Assuming the leg's longitudinal axis is z, then its Cartesian stiffness matrix $\boldsymbol{K}_{p|\mathrm{L}}$ relates the forces, torques, and linear and angular displacements at point p as follows:

$$\begin{bmatrix} f_x \\ f_y \\ f_z \\ m_\phi \\ m_\theta \\ m_\psi \end{bmatrix} = \underbrace{\begin{bmatrix} k_{\text{shear}} & k_{xy} & k_{xz} & k_{x\phi} & k_{x\theta} & k_{x\psi} \\ k_{yx} & k_{\text{shear}} & k_{yz} & k_{y\phi} & k_{y\theta} & k_{y\psi} \\ k_{zx} & k_{zy} & k_{\text{axial}} & k_{z\phi} & k_{z\theta} & k_{z\psi} \\ k_{\phi x} & k_{\phi y} & k_{\phi z} & k_{\text{bending}} & k_{i,\phi\theta} & k_{\phi\psi} \\ k_{\theta x} & k_{\theta y} & k_{\theta z} & k_{\theta\phi} & k_{\text{bending}} & k_{\theta\psi} \\ k_{\psi x} & k_{\psi y} & k_{\psi z} & k_{i,\psi\phi} & k_{\psi\theta} & k_{\text{torsion}} \end{bmatrix}}_{\boldsymbol{K}_{p|\mathrm{L}}} \cdot \begin{bmatrix} \delta_x \\ \delta_y \\ \delta_z \\ \delta_\phi \\ \delta_\theta \\ \delta_\psi \end{bmatrix} \tag{19}$$

For compactness, $\boldsymbol{K}_{p|\mathrm{L}}$ can be rewritten as in Eq. (20):

$$\boldsymbol{K}_{p|\mathrm{L}} = \begin{bmatrix} \boldsymbol{K}_{\mathrm{tt}} & \boldsymbol{K}_{\mathrm{tr}} \\ \boldsymbol{K}_{\mathrm{rt}} & \boldsymbol{K}_{\mathrm{rr}} \end{bmatrix}, \tag{20}$$

where $\boldsymbol{K}_{\mathrm{tt}}$ is the translational stiffness submatrix, $\boldsymbol{K}_{\mathrm{rr}}$ is the rotational stiffness submatrix, and $\boldsymbol{K}_{\mathrm{tr}}$ and $\boldsymbol{K}_{\mathrm{rt}}$ are coupling stiffness submatrices.

The starting point of the development is the output of a modal analysis of a single hexapod actuator, obtained from a high-dimensional finite element model. For this analysis, the 50 first normal modes were considered. For each of these modes, the analysis provides their modal characteristics, i.e. their natural frequency, effective mass fraction, generalized mass and generalized stiffness coefficients. The effective mass fraction indicates the mode's influence (i.e., in which translational or rotational direction it acts) and importance (fraction of total mass moved when excited at the frequency). The FEM output also contains the 6-by-6 global mass matrix of the actuator $\boldsymbol{M}_{h|\mathrm{L}}$, expressed at a reference point h in the actuator frame $\{\mathrm{L}\}$. This mass matrix is composed of the 3-by-3 mass and moment of inertia submatrices as diagonal blocks, and two 3-by-3 off-diagonal submatrices.

Klimchik et al.[12] showed that the Cartesian stiffness matrix of a hexapod platform only includes the traction/compression terms of the actuator modes. Since the same 6-3 hexapod geometry is considered in their study, these results provide a certain level of confidence and are used as a first modeling assumption for this article. This means that in the modal results, the axial modes are kept while the remaining ones (including bending and torsion modes) are ignored. For the studied actuator design, the effective mass fraction of the first axial mode is 100%. This means that considering this mode alone enables it to capture the traction/compression behavior of the actuator. The next step consists in computing the Cartesian 6-by-6 stiffness matrix $\boldsymbol{K}_{p|\mathrm{L}}$ of the actuator corresponding to this mode. The FEM output provides the axial mode's generalized stiffness, which is the axial stiffness expressed in the modal coordinates. This stiffness is needed in the actuator frame, which is the frame where the global mass matrix of the actuator $\boldsymbol{M}_{h|\mathrm{L}}$ is expressed. The idea is to compute the eigenvector $\boldsymbol{\phi}_{axial}$ of the mode to relate these two frames:

$$k_{\text{axial,gen}} = \boldsymbol{\phi}_{\text{axial}}^{\top}\, \boldsymbol{K}_{h|\mathrm{L}}\, \boldsymbol{\phi}_{\text{axial}} \tag{21}$$

In the FEM output, the eigenvector is normalized such that the generalized mass is unitary as follows:

$$1 = \boldsymbol{\phi}_{axial}^{\top}\, \boldsymbol{M}_{h|\mathrm{L}}\, \boldsymbol{\phi}_{axial} \tag{22}$$

Solving Eq. (22) provides the eigenvector $\boldsymbol{\phi}_{axial}$, and in turn the 6-by-6 Cartesian stiffness matrix $\boldsymbol{K}_{h|\mathrm{L}}$ of the actuator by manipulating Eq. (21). A last step is needed to express this stiffness matrix at point p. To do so, the following transportation matrix $\boldsymbol{\tau}_{hp}$ is used:

$$\boldsymbol{\tau}_{hp} = \begin{bmatrix} \boldsymbol{I}_3 & \boldsymbol{0}_3 \\ -[\boldsymbol{r}_{hp}]_\times & \boldsymbol{I}_3 \end{bmatrix}, \tag{23}$$

where $\boldsymbol{I}_3$ is the 3-by-3 identity matrix, $\boldsymbol{0}_3$ is the 3-by-3 null matrix and $\boldsymbol{r}_{hp}$ is the vector from h to p. Then, the Cartesian stiffness of an individual actuator with respect to p is:

$$\boldsymbol{K}_{p|\mathrm{L}} = \boldsymbol{\tau}_{hp}^{\top}\, \boldsymbol{K}_{h|\mathrm{L}}\, \boldsymbol{\tau}_{hp} \tag{24}$$

DOI: 10.13009/EUCASS2023-374

3.3.2 Aggregation of the individual actuator stiffness matrices

In this section, the individual stiffness matrices are aggregated. The subscript i is added in the stiffness matrix obtained in Eq. (24) to refer to the leg i of the hexapod, leading to $\boldsymbol{K}_{i,p_i|\mathrm{L_i}}$.

As the stiffness properties of each actuator leg is expressed in a Cartesian frame, this allows to assemble the contributions from all the legs using the mechanism's geometric parameterization to form the global Cartesian stiffness matrix of the hexapod. It consists in expressing all the individual Cartesian stiffness matrices in the platform frame {P} and at the same point p in order to add them. This modular process is analogous to the one used by Alazard et al.[2] to assemble linear dynamic models for multi-body-systems.

First, the i-th leg's Cartesian stiffness matrix $\boldsymbol{K}_i$ can be expressed in the hexapod's platform frame R_P using the direct cosine matrix ${}^{P}\boldsymbol{R}_{L_i}$ computed in Eq. (7):

$$\boldsymbol{K}_{i,p_i|\mathrm{P}} = {}^{P}\boldsymbol{R}_{L_i}\, \boldsymbol{K}_{i,p_i|\mathrm{L_i}}\, {}^{P}\boldsymbol{R}_{L_i}{}^{\top} \tag{25}$$

Now that the i-th leg's Cartesian stiffness matrix is expressed in the platform frame {P}, it needs to be transported from the i-th junction point p_i to the origin p of the platform frame {P}. To do so, the transportation matrix introduced in Eq. (23) applied to the vector $\boldsymbol{r}_{p_i p}$ is used.

$$\boldsymbol{K}_{i,p|\mathrm{P}} = \boldsymbol{\tau}_{p_i p}{}^{\top}\, \boldsymbol{K}_{i,p_i|\mathrm{P}}\, \boldsymbol{\tau}_{p_i p} \tag{26}$$

Finally, the six individual Cartesian stiffness matrices are added to form the global hexapod stiffness matrix:

$$\boldsymbol{K}_{\mathrm{P}} = \sum_{i=0}^{6} \boldsymbol{K}_{i,p|\mathrm{P}} \tag{27}$$

The stiffness matrix has full-rank, which means that the considered geometry has a stable behavior to an external wrench input. It does not allow any free rotation around any axis.

4. Hexapod equivalent stiffness verification and validation

4.1 Verification and validation concept

In this work, the verification of the equivalent stiffness matrix ensures that the oscillations' amplitudes and frequencies obtained analytically in section 3.2 are accurate. On the other hand, The validation shall assess the validity of the equivalent stiffness matrix by confronting it to a higher fidelity model of the hexapod.

Verification model: A verification model composed of two bodies is derived, with the equivalent stiffness matrix as a 6-dof-link in-between. The temporal response of this verification model to external forces and torques impulses are simulated, and the oscillations' amplitudes and frequencies are compared to the expected analytical ones, and low relative errors (<0.001%) are expected.

Verification simulator: For this verification, it is essential to use a dynamics tool where the hexapod equivalent stiffness matrix computed in Eq. (27) can be used as a 6-dof-link between the two bodies. Since the equivalent stiffness matrix is not necessarily diagonal, this link must enable stiffness coupling between the different axes. The verification is performed on an Airbus in-house tool for multi-body dynamics, which can model these effects to the required level of detail.

Validation model: Although a detailed FEM of one actuator is available, no model of the whole hexapod was developed yet. Thus a validation model with a physical representation of the six actuators is derived. It is composed of two bodies, with a hexapod model containing the six flexible actuators in between. The temporal response of this validation model to external forces and torques are simulated, and the oscillations' amplitudes and frequencies are compared to the expected analytical ones. We consider the validation successful if the relative errors of amplitude and frequency are below 10%

Validation simulator: For the validation, it is essential to use a simulation tool where the hexapod mechanism can be modeled with high fidelity. Hence, a tool that can solve differential-algebraic equations (DAEs), with the possibility of modeling flexible bodies, is required. Simscape Multibody was selected for the model validation. It is a commercially available non-linear multi-body simulation tool integrated in the Matlab/Simulink software. We selected Simscape Multibody because it can solve DAEs and is integrated in the MATLAB/Simulink software framework. Thus, it enables an accurate but simple modeling of the hexapod in a common and known environment for performing simulations.

The verification and validation concept is summed up in Figure 3. The direct modeling process presented before is used in a hexapod case-study, described in Section 4.2, and the verification and validation results shown respectively in Section 4.3 and 4.4.

DOI: 10.13009/EUCASS2023-374

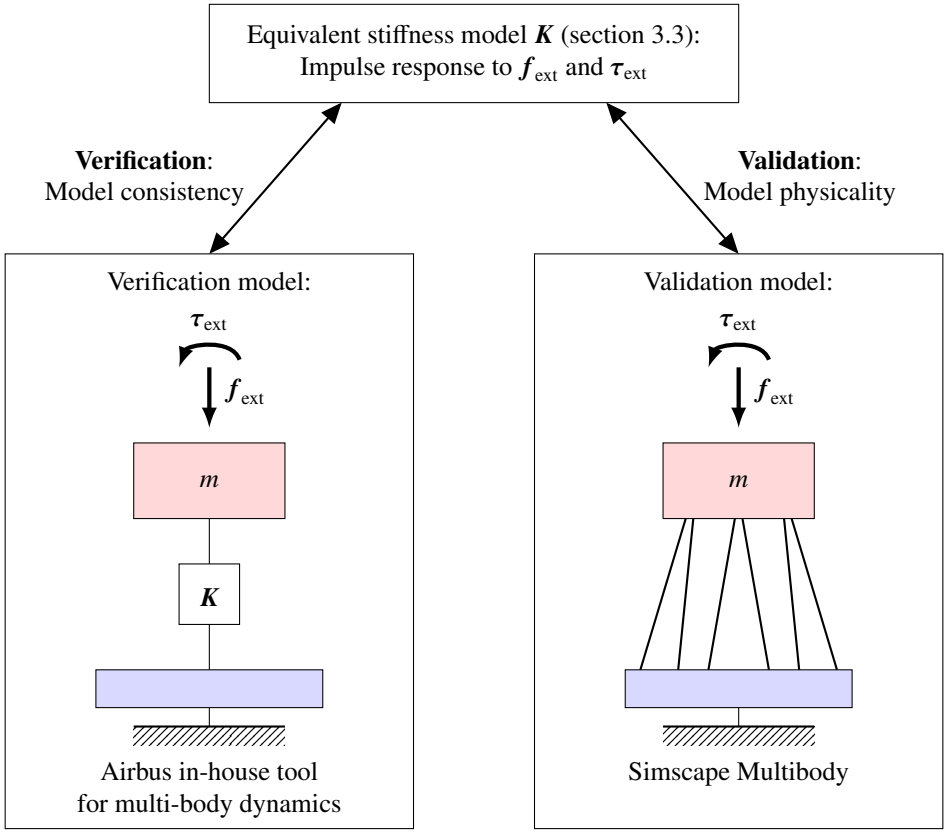

Figure 3: Verification and validation concept

4.2 Case-study model

A case study based on the hexapod geometry originally foreseen for the ATHENA spacecraft[1,9] is used to exemplify the approach (see Table A1 in Appendix A). The maximum actuator length is considered since it corresponds to the lowest stiffness, and thus to the worst case regarding the mechanism flexibility. An alternative actuator is considered for the stiffness model verification and validation. The considered actuator is a beam, whose mechanical properties can be found in Table A1. The mass and inertia properties of the platform are adapted to these alternative actuators and are also provided in Table A1.

These characteristics lead to an axial term of the actuator Cartesian stiffness matrix of $k_{\text{axial}} = 1.0219\times10^{7}\ \text{N}\cdot\text{m}^{-1}$. The process from section 3.3.2 is now followed to aggregate these individual actuator stiffness matrices, leading to the following equivalent stiffness matrix for the hexapod mechanism:

$$\boldsymbol{K} = \begin{bmatrix} 0.6246 & 0 & 0 & 0 & -0.4130 & 0 \\ 0 & 0.6246 & 0 & 0.4130 & 0 & 0 \\ 0 & 0 & 4.8822 & 0 & 0 & 0 \\ 0 & 0.4130 & 0 & 3.5152 & 0 & 0 \\ -0.4130 & 0 & 0 & 0 & 3.5152 & 0 \\ 0 & 0 & 0 & 0 & 0 & 1.6591 \end{bmatrix} \cdot 10^{7} \tag{28}$$

The hexapod natural frequency vector $\boldsymbol{f}$ depends on the stiffness and mass and inertia properties. It is obtained by following the process of Eq. (10).

$$\boldsymbol{f} = \frac{\boldsymbol{\omega}}{2\pi} = \begin{bmatrix} f_1 & f_2 & f_3 & f_4 & f_5 & f_6 \end{bmatrix}^{\top} \tag{29}$$

It takes the following numerical values:

$$\boldsymbol{f} = \begin{bmatrix} 120 & 120 & 352 & 400 & 400 & 193 \end{bmatrix}^{\top} \text{Hz} \tag{30}$$

DOI: 10.13009/EUCASS2023-374

The amplitude vector in the eigenbasis depends on the input wrench $\boldsymbol{w}_{\text{ext}}$ acting on the hexapod's platform, which is an impulse vector composed of the following elements.

$$\boldsymbol{w}_{\text{ext}} = \begin{bmatrix} f_x & f_y & f_z & \tau_x & \tau_y & \tau_z \end{bmatrix}^\top \tag{31}$$

The previous impulse vector, the amplitude vector $\boldsymbol{\alpha}$ from Eq. (14) is function of the parameters in brackets:

$$\boldsymbol{\alpha} = \begin{bmatrix} \alpha_1(\omega_1, f_x, \tau_y) \\ \alpha_2(\omega_2, f_y, \tau_x) \\ \alpha_3(\omega_3, f_z) \\ \alpha_4(\omega_4, f_y, \tau_x) \\ \alpha_5(\omega_5, f_x, \tau_y) \\ \alpha_6(\omega_6, \tau_z) \end{bmatrix} \tag{32}$$

Keeping the notations from Eq. (13), the solution can be expressed in the Eigenbasis in function of the input forces and torques impulses as follows:

$$\tilde{\boldsymbol{X}}(t) = \begin{bmatrix} \alpha_1(\omega_1, f_x, \tau_y)\sin(\omega_1 t) \\ \alpha_2(\omega_2, f_y, \tau_x)\sin(\omega_2 t) \\ \alpha_3(\omega_3, f_z) \quad \sin(\omega_3 t) \\ \alpha_4(\omega_4, f_y, \tau_x)\sin(\omega_4 t) \\ \alpha_5(\omega_5, f_x, \tau_y)\sin(\omega_5 t) \\ \alpha_6(\omega_6, \tau_z) \quad \sin(\omega_6 t) \end{bmatrix} \tag{33}$$

The linear and angular solutions along each axis of the platform frame {P} can be expressed in function of the input forces and torques impulses as derived in Eq. (18). These solutions are given in Eq. (34).

$$\boldsymbol{x}(t) = \begin{bmatrix} P_{11}\ \alpha_1(\omega_1, f_x, \tau_y)\sin(\omega_1 t) + P_{15}\ \alpha_5(\omega_5, f_x, \tau_y)\sin(\omega_5 t) \\ P_{22}\ \alpha_2(\omega_2, f_y, \tau_x)\sin(\omega_2 t) + P_{24}\ \alpha_4(\omega_4, f_y, \tau_x)\sin(\omega_4 t) \\ P_{33}\ \alpha_3(\omega_3, f_z) \quad \sin(\omega_3 t) \\ P_{42}\ \alpha_2(\omega_2, f_y, \tau_x)\sin(\omega_2 t) + P_{44}\ \alpha_4(\omega_4, f_y, \tau_x)\sin(\omega_4 t) \\ P_{51}\ \alpha_1(\omega_1, f_x, \tau_y)\sin(\omega_1 t) + P_{55}\ \alpha_5(\omega_5, f_x, \tau_y)\sin(\omega_5 t) \\ P_{66}\ \alpha_6(\omega_6, \tau_z) \quad \sin(\omega_6 t) \end{bmatrix} \tag{34}$$

It can be observed that for forces and torques along the $\boldsymbol{z}_P$-axis (i.e. third and sixth row), the solutions are exact sine waves. In the other cases, there is a coupling behavior between the $\boldsymbol{x}_P$ and $\boldsymbol{z}_P$ axes. The solutions are the addition of two sine waves at different frequencies and amplitudes, which do not result in a sine waves.

4.3 Model verification on an Airbus in-house multi-body dynamics tool

In this section, the analytical dynamics formulation and solution from section 3.1 is verified. The verification model presented in section 4 is applied to the case-study from section 4.2. Hence, the stiffness behavior of the link is represented by the equivalent stiffness matrix from Eq. (28). The platform is subjected to different impulsive input forces and torques and the time response of the platform position and orientation is simulated. The expected response characteristics are computed beforehand following the method from section 3.2. They consist in a combination of oscillations, whose amplitudes and frequencies are known (see Eq. (34)). The test scenario is summarized in Table A2 in Appendix A.

The equivalent model is simulated and the amplitude and frequency of its oscillations are compared to the theoretical ones. A fixed-step solver was used, with a frequency 100 times higher than the highest dynamics frequency that needs to be observed. The temporal responses for the first case f_x are shown. Figure 4 shows the linear response about the $\boldsymbol{x}_P$-axis, while Figure 5 shows the angular response about the $\boldsymbol{y}_P$-axis.

For all the impulses shown in Table A2, the amplitude relative error mean was always between 10^{-6} and 10^{-7} and its relative error variance between 10^{-14} to 10^{-17} (and for the frequency, both metrics are 0 for all cases). The zero-variances were expected, since the analytical model is completely deterministic. Furthermore, the low relative errors (mean values $< 10^{-6}$) show that the dynamic model with the equivalent stiffness matrix computed in Eq. (27) has been correctly solved.

DOI: 10.13009/EUCASS2023-374

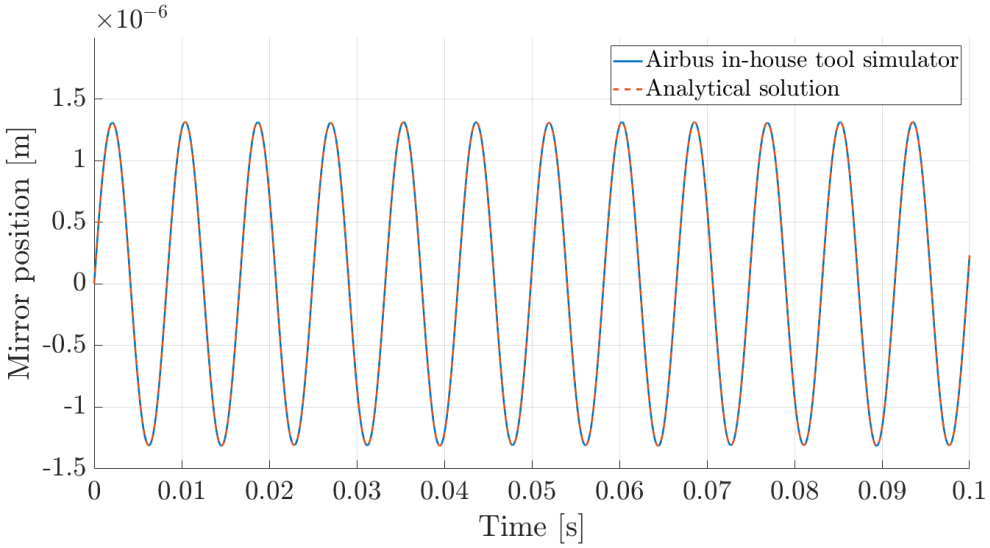

Figure 4: Response to impulse input f_x about $\mathbf{x}_P$-axis

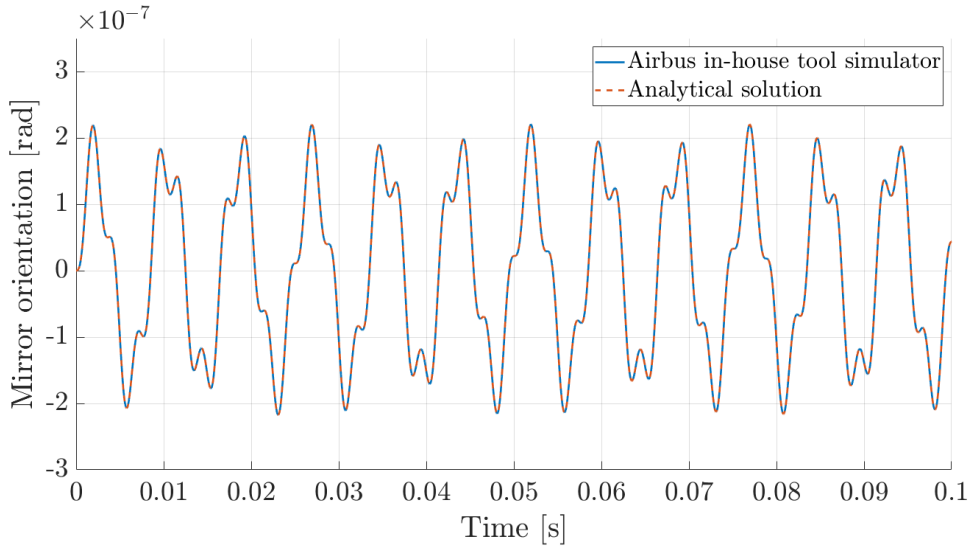

Figure 5: Response to impulse input f_x about $\mathbf{y}_P$-axis

4.4 Model validation on Simscape Multibody

After verifying the analytical formulation and solution of the equivalent stiffness model, its physical validity must be assessed. To this end, the case-study model from Section 4.2 has been created on Simscape Multibody. This validation model serves as reference case. The same test-case scenario as the one in Table A2 was simulated, and the resulting responses were compared to the theoretical ones.

For the primary responses (first line for each impulsive input in Table A2), the amplitudes of the equivalent model differ from the non-linear ones by less than 10^{-4} in mean relative error. There is a light frequency shift between the models, with a relative error of 10^{-4} for all the cases. These frequency shifts are due to the fact that the model has more stiffness in Simscape than the equivalent one with the axial stiffness only. This leads to greater natural frequencies than the theoretical model. The amplitude mean relative error of the induced responses is about 1% for all the cases. These results further confirm that the assumption of considering the axial stiffness only in the actuators[12, 17, 20] is consistent.

The temporal responses for the first case f_x are shown. Figure 6 shows the primary linear response about the $\boldsymbol{x}_P$-axis, while Figure 7 shows the induced angular response about the $\boldsymbol{y}_P$-axis.

DOI: 10.13009/EUCASS2023-374

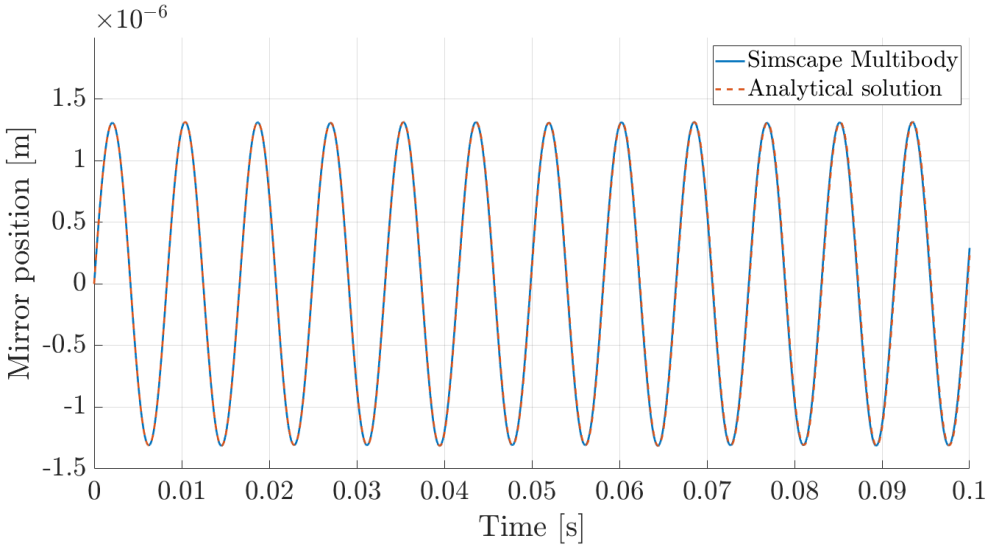

Figure 6: Response to impulse input f_x about $\mathbf{x}_P$-axis

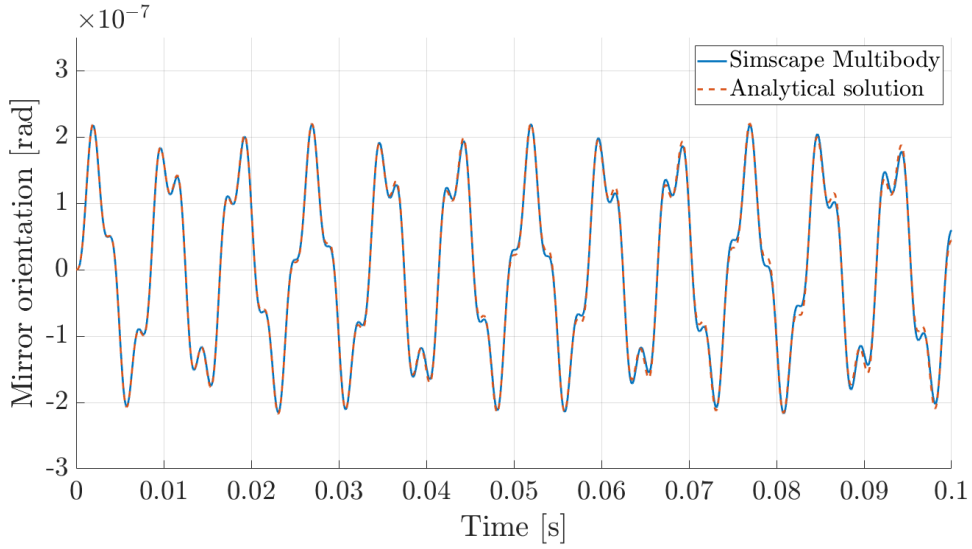

Figure 7: Response to impulse input f_x about $\mathbf{y}_P$-axis

For the case study, the actuator-to-mirror mass ratio is actually around 1%, and the equivalent stiffness model does not take into account the actuators' mass. In order to verify the validity of the model for this ratio, the actuators' mass is added in the Simscape validation model and the impact on the hexapod's natural frequencies is assessed. The mass almost has no impact on the linear frequencies since the relative error stays by 10^{-4}. However, the angular frequencies decrease with the mass, and the relative error in frequency increases from 10^{-4} to 1% for the 1% actuator-to-mirror mass ratio.

For a better visualization of the impact on the frequencies, the Bode diagrams of the linearized systems are drawn. The same transfer as Figures 6 and 7 are shown for different mass ratios in the Simscape model: 0.01%, which corresponds to a negligible actuator mass, 0.1% and 1%, which corresponds to the case study. Figure 8 focuses on the linear frequency and shows that the mass has almost no effect on this frequency. On the other hand, the shift in frequency can be observed when focusing on the induced angular frequency (see Figure 9).

DOI: 10.13009/EUCASS2023-374

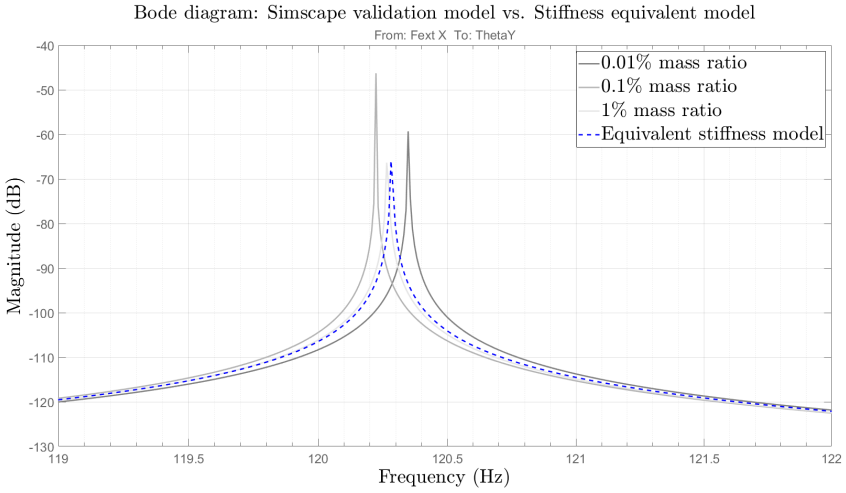

Figure 8: Transfer from f_x to mirror orientation about $\mathbf{y}_P$-axis: focus on linear frequency

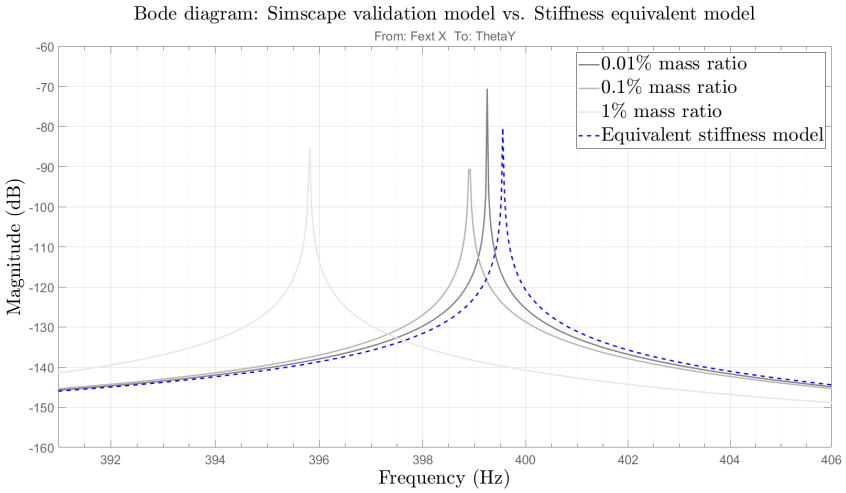

Figure 9: Transfer from f_x to mirror orientation about $\mathbf{y}_P$-axis: focus on induced angular frequency

5. Conclusions

In this article, the derivation of a hexapo stiffness model has been studied. This model consists of an equivalent Cartesian stiffness matrix of the hexapod. This stiffness matrix relates the forces and torques applied on the hexapod's platform to its linear and angular displacements. A process to assemble stiffness properties of individual elements of a mechanism was established and implemented.

The above process was applied to a hexapod study-case. A verification simulator using an Airbus in-house tool for multi-body dynamics was derived. The verification model is based on the approximation of the interconnection between the two bodies, which is the equivalent stiffness matrix of the study-case hexapod. A validation simulator using Simscape Multibody was derived. The validation model is based on the physical description of the interconnection, which is the set of six actuators of the study-case hexapod.

The verification assesses the consistency of the equivalent stiffness matrix of the study-case hexapod against the results from the verification simulator. The validation assesses the physicality of this equivalent stiffness matrix against the results from the validation simulator.

Results show that the proposed methodology leads to both an accurate and physical equivalent stiffness model. Indeed, the verification shows small relative errors in terms of amplitude ($< 10^{-6}$) and no error in the frequency of the oscillations. Further, the ease of implementation of the approach means that it satisfies the transparent and

DOI: 10.13009/EUCASS2023-374

clear requirements by industry of any algorithm that must be deployed on-board. The validation results show that the equivalent stiffness model is valid under the modeling assumptions with small relative errors in amplitude (10^{-4}) and a shift in frequency with a relative error of 10^{-4}. They also show that the equivalent stiffness model stays physical for small actuator-to-payload ratio (always < 1%).

Thus, the equivalent stiffness model of the hexapod enables approximating the flexible modes of such a mechanism, without the need of deriving non-linear dynamics formulation, nor a detailed FEM model of the mechanism. The linear and angular responses to an impulsive input were provided as a sum of sine waves, which individual amplitudes and frequencies are known. In addition, this equivalent stiffness model is linear and parameterized with the actuator's properties and the hexapod's geometry. Thus, this model is easily extensible to linear uncertainties, providing a solid base for a later control design.

References

[1] ATHENA CDF Study Report: CDF-150(A). Technical report, European Space Agency, 2014.

[2] D. Alazard, C. Cumer, and K. Tantawi. Linear Dynamic Modeling of Spacecraft with Various Flexible Appendages and On-Board Angular Momentums. In *ESA GNC 2008*, 2021.

[3] Daniel Alazard, José Alvaro Perez Gonzalez, Thomas Loquen, and Christelle Cumer. Two-input two-output port model for mechanical systems. 2015.

[4] Jawhar Chebbi, Vincent Dubanchet, José Alvaro Perez Gonzalez, and Daniel Alazard. Linear dynamics of flexible multibody systems : a system-based approach. *Multibody System Dynamics*, 41(1):75–100, September 2017.

[5] Bhaskar Dasgupta and T.S. Mruthyunjaya. A newton-euler formulation for the inverse dynamics of the stewart platform manipulator. *Mechanism and Machine Theory*, 33(8):1135–1152, 1998.

[6] W. Q. D. Do and D. C. H. Yang. Inverse dynamic analysis and simulation of a platform type of robot. *J. Field Robotics*, 5:209–227, 1988.

[7] A. Finozzi, F. Sanfedino, and D. Alazard. Parametric sub-structuring models of large space truss structures for structure/control co-design. *Mechanical Systems and Signal Processing*, 180:109427, 2022.

[8] Zheng Geng, Leonard S. Haynes, James D. Lee, and Robert L. Carroll. On the dynamic model and kinematic analysis of a class of stewart platforms. *Robotics and Autonomous Systems*, 9(4):237–254, 1992.

[9] S. Goerries. Athena space telescope: Line of sight control with a hexapod in the loop. *MSc thesis, KTH Royal Institute Of Technology*, 2017.

[10] Youhong Gong. Design analysis of a stewart platform for vehicle emulator systems. *MSc thesis, Massachusetts Institute of Technology*, 11 1992.

[11] Nicolas Guy, Daniel Alazard, Christelle Cumer, and Catherine Charbonnel. Dynamic modeling and analysis of spacecraft with variable tilt of flexible appendages. *Journal of Dynamic Systems, Measurement, and Control*, 136:021020, 03 2014.

[12] Alexandr Klimchik, Anatol Pashkevich, Stéphane Caro, and Damien Chablat. Stiffness matrix of manipulators with passive joints: Computational aspects. *IEEE Transactions on Robotics*, 28(4):955–958, aug 2012.

[13] J.D. Lee and Z. Geng. A dynamic model of a flexible stewart platform. *Computers and Structures*, 48(3):367–374, 1993.

[14] Mou Li, Yao Zhang, Youyi Wang, Quan Hu, and Rui Qi. The pointing and vibration isolation integrated control method for optical payload. *Journal of Sound and Vibration*, 438:441–456, 2019.

[15] Antonio Mendes Lopes and Fernando Gomes de Almeida. Dynamic model of a 6-dof parallel manipulator using the generalized momentum approach. In *Proceedings ENOC'08*, 2008.

[16] F. Landis Markley and John L. Crassidis. *Attitude Kinematics and Dynamics*, pages 67–122. Springer New York, New York, NY, 2014.

DOI: 10.13009/EUCASS2023-374

[17] Carlo Menon, Rocco Vertechy, Mihaly Markot, and Vincenzo Parenti Castelli. Geometrical optimization of parallel mechanisms based on natural frequency evaluation: Application to a spherical mechanism for future space applications. *Robotics, IEEE Transactions on*, 25:12 – 24, 03 2009.

[18] Vincenzo Parenti-Castelli and Raffaele Di Gregorio. Closed-form solution of the direct kinematics of the 6–3 type stewart platform using one extra sensor. *Meccanica*, pages 705–714, 1996.

[19] Anatol Pashkevich, Alexandr Klimchik, Stéphane Caro, and Damien Chablat. Cartesian stiffness matrix of manipulators with passive joints: Analytical approach. *IEEE International Conference on Intelligent Robots and Systems*, 07 2011.

[20] V.T. Portman, B.-Z. Sandler, and E. Zahavi. Rigid 6/spl times/6 parallel platform for precision 3-d micromanipulation: theory and design application. *IEEE Transactions on Robotics and Automation*, 16(6):629–643, 2000.

[21] Francesco Sanfedino, Daniel Alazard, Valérie Pommier-Budinger, Alexandre Falcoz, and Fabrice Boquet. Finite element based n-port model for preliminary design of multibody systems. *Journal of Sound and Vibration*, 415:128–146, 2018.

[22] Francesco Sanfedino, Gabriel Thiébaud, Daniel Alazard, Nicola Guercio, and Nicolas Deslaef. Advances in fine line-of-sight control for large space flexible structures. *Aerospace Science and Technology*, 130:107961, 2022.

[23] Se-Kyong Song and Dong-Soo Kwon. New methodology for the forward kinematics of 6-dof parallel manipulators using tetrahedron configurations. In *Proceedings 2001 ICRA. IEEE International Conference on Robotics and Automation (Cat. No.01CH37164)*, volume 2, pages 1307–1312 vol.2, 2001.

[24] Jiegao Wang, Clément Gosselin, and Li Cheng. Modeling and simulation of robotic systems with closed kinematic chains using the virtual spring approach. *Multibody System Dynamics*, 7:145–170, 2002.

DOI: 10.13009/EUCASS2023-374

A. Appendix

Table A1: Hexapod mechanism geometrical configuration

Category	Parameter	Name	Value	Unit
Hexapod geometry	Radius on platform side[9]	r_{P}	1200	mm
	Radius on base side[9]	r_{B}	1320	mm
	Base angle from base center[9]	β	26	deg
	Actuator length (i.e. fully deployed)[9]	l	685	mm
	Distance between two nearby base points	s	297	mm
	Base angle from platform point	α	51	deg
	Distance between middle of base length and r_P	d	86	mm
	Projection of platform point to base	h_i	611	mm
	Leg angle from vertical	γ	27	deg
Hexapod's platform	Mass	m	10	kg
	Matrix of Inertia	$\mathcal{J}$	$\begin{bmatrix} 5.62 & 0 & 0 \\ 0 & 5.62 & 0 \\ 0 & 0 & 11.25 \end{bmatrix}$	kg·m^2
Actuator properties	Young modulus	E	70	GPa
	Poisson's ratio	ν	0.33	-
	Cross-section	A	1×10^{-4}	m^2

Table A2: Expected platform responses: combination of primary and secondary oscillations

Input impulse	Output oscillations	Primary oscillations		Secondary oscillations	
		Amplitude	Frequency	Amplitude	Frequency
f_x = 0.01 N	Linear, $\boldsymbol{x}_P$	$P_{11}\ \alpha_1(\omega_1, f_x, \tau_y)$	f_1	$P_{15}\ \alpha_5(\omega_5, f_x, \tau_y)$	f_5
	Angular, $\boldsymbol{y}_P$	$P_{51}\ \alpha_1(\omega_1, f_x, \tau_y)$	f_1	$P_{55}\ \alpha_5(\omega_5, f_x, \tau_y)$	f_5
f_y = 0.01 N	Linear, $\boldsymbol{y}_P$	$P_{22}\ \alpha_2(\omega_2, f_y, \tau_x)$	f_2	$P_{24}\ \alpha_4(\omega_4, f_y, \tau_x)$	f_4
	Angular, $\boldsymbol{x}_P$	$P_{42}\ \alpha_2(\omega_2, f_y, \tau_x)$	f_2	$P_{44}\ \alpha_4(\omega_4, f_y, \tau_x)$	f_4
f_z = 0.01 N	Linear, $\boldsymbol{z}_P$	$P_{33}\ \alpha_3(\omega_3, f_z)$	f_3	-	-
τ_x = 0.01 N·m	Angular, $\boldsymbol{x}_P$	$P_{44}\ \alpha_4(\omega_4, f_y, \tau_x)$	f_4	$P_{42}\ \alpha_2(\omega_2, f_y, \tau_x)$	f_2
	Linear, $\boldsymbol{y}_P$				
τ_y = 0.01 N·m	Angular, $\boldsymbol{y}_P$	$P_{55}\ \alpha_5(\omega_5, f_x, \tau_y)$	f_5	$P_{51}\ \alpha_1(\omega_1, f_x, \tau_y)$	f_1
	Linear, $\boldsymbol{x}_P$				
τ_z = 0.01 N·m	Angular, $\boldsymbol{z}_P$	$P_{66}\ \alpha_6(\omega_6, \tau_z)$	f_6	-	-